Univerzita Palackého v Olomouci
Přírodovědecká fakulta
Společná laboratoř optiky UP a FZÚ AV ČR v Olomouci

BAKALÁŘSKÁ PRÁCE

Characterization of CCD sensors for the LSST

Autor: Jan Smolka

Studijní program: B1701 Fyzika

Studijní obor: 1701R030 Přístrojová fyzika

Forma studia: Prezenční

Vedoucí práce: RNDr. Michael Prouza, Ph.D.

Termín odevzdání práce: 14. 5. 2018

Prohlašuji, že jsem předloženou bakalářskou práci vypracoval samostatně pod vedením RNDr. Michaela Prouzy, Ph.D. a že jsem použil zdrojů, které cituji a uvádím v seznamu.

V Olomouci dne 14. 5. 2018 ...…….....

Jan Smolka

Děkuji RNDr. Michaelu Prouzovi, Ph. D. a Mgr. Martinu Blažkovi, Ph. D. za kvalifikované vedení mé bakalářské práce, cenné rady a odbornou pomoc, kterou mi věnovali.

Bibliografická identifikace:

Jméno a příjmení autora	Jan Smolka
Název práce	Charakterizace CCD čipů pro přehlídkový dalekohled LSST
Typ práce	Bakalářská
Pracoviště	Společná laboratoř optiky
Vedoucí práce	RNDr. Michael Prouza, Ph.D..
Rok obhajoby práce	2018
Abstrakt	Přehlídkový dalekohled LSST je plánovaným největším a nejvýkonnějším přístrojem pro studium "hlubokého vesmíru", který bude zprovozněn v roce 2022. Dalekohled nasnímá celou pozorovatelnou oblohu za pouhé tři noci do dosud bezprecendentní hloubky. Bude extrémně citlivý na jakékoli proměnné zdroje a za 10 let svého provozu se očekává, že zmapuje například polohu 3 miliard galaxií, objeví 250 tisíc supernov, nebo se bude věnovat sledování asteroidů potenciálně ohrožujících Zemi. V současné době již probíhají práce na jeho konstrukci, Fyzikální ústav AV ČR se podílí například na charakterizaci CCD čipů jeho mozaikové kamery, čemuž by se měla věnovat i navržená bakalářská práce.
Klíčová slova	sky survey, Large Synoptic Survey Telescope, LSST, Charge-coupled device, CCD, CCD characterization, CCD properties
Počet stran	53
Počet příloh	0
Jazyk	Anglický

Bibliographical identification:

Autor's first name and surname	Jan Smolka
Title	Characterization of CCD sensors for the LSST telescope
Type of thesis	Bachelor
Department	Joint labratory of optics
Supervisor	RNDr. Michael Prouza, Ph.D.
The year of presentation	2018
Abstract	LSST is the largest and most powerful deep-space exploration device that will be operational in 2022. The telescope will capture the entire observable sky in just three nights, to scan deepest area of the universe . It will be extremely sensitive to any variable sources, and in 10 years of its operation it is expected to map, for example, the location of 3 billion galaxies, to discover 250,000 supernovae, or to track asteroids potentially threatening the Earth. At present, work on its construction is under way, the Institute of Physics of the Academy of Sciences of the Czech Republic participates, for example, in the characterization of CCD chips in its mosaic camera, which should also be devoted to the proposed bachelor thesis.
Keywords	sky survey, Large Synoptic Survey Telescope, LSST, Charge-coupled device, CCD, CCD characterization, CCD properties
Number of pages	53
Number of appendices	0
Language	English

Table of content

1 Introduction

Human race always wanted to see beyond the limits and to explore the unknown. We built the devices around the world and even sent them into space. The Large Survey Synoptic Telescope (LSST) is a big step for whole humankind. The LSST is going to be the largest telescope in the world that allows to explore whole night sky during three nights and helps us reveal its secrets. The LSST is going to be used for 10 years. It is a long time for achieving big discoveries and breakthroughs. The most important part of the LSST is Charge Couple Device (CCD). The CCD is a basic element that used is for imaging in astronomy. In everyday electronics CCD, is pushed out by cheaper Complementary Metal–Oxide–Semiconductor (CMOS) sensors but in the astronomy use of CCD has special a place and it is used in most astronomical projects. But before putting the CCDs into LSST they need to be tested. The LSST has the main laboratory in Brookhaven (USA), where is large cleanroom laboratory that contains 8 testing stands for CCD testing, but it has also partnered laboratories around the world for CCD characterization. One of those resides in Prague at Institute of Physics (IoP) at Czech Academy of Science (CAS) here the laboratory is fully equipped and prepared for CCD testing and measuring.

In this thesis, my work is to help to develop the laboratory for future CCD testing, learn to get CCD characterization methods and be familiar with the LSST project.
For laboratory development, I was focusing on of the testing behaviour of vacuum chamber during cooling down a process and learning about CCD characterization. Describing of the behaviour of the vacuum chamber was crucial for future measurements and helped to understand more possible states that could happen. To achieve that, it was important to understand each part of the device and it was necessary to make technical intervention to get the results. The Second part was to learn methods for CCD characterization and to understand the aspects its. First of all I had to learn about CCDs, how they work and about their properties.
For CCD characterization it is important to understand defects that can appear during measurement and how they can be removed or decreased. This involves a collection of data and their deep analysis. It is necessary to have special equipment and to know

how to work with it. Special equipment involves vacuum chamber, temperature controller Cryocon, Dewar flasks, Archon and software frameworks. Learning how to work with each testing tool was also part of my task. I had to learn how to manipulate with the equipment and how to understand how each part works.
In this thesis, I had to learn about the LSST project especially about his science goals that the LSST want to achieve in future and about the CCD camera construction with a high-end resolution that will be mounted on LSST.

The thesis is divided in two main parts. First part is the theoretical part about LSST and CCD sensors (Chapters 1 – 3). The second part then describes my own measurements and experiments and discusses their results (4-6).

2 Large Synoptic Survey Telescope

The Large Synoptic Survey Telescope (LSST) is a ground-based telescope that consists of wide (Fig. 2) – field resolution camera and his location is in northern Chile on Cerro Pachón (Fig. 1). This project belongs to National Science Foundation (NSF) of USA that shares partnership with the Department of Energy (DOE) Office of Science. LSST is designed for imaging of significant fractions of the night sky. This imaging should help us to extend our knowledge of the universe. The LSST has a wide range of goals in astronomy, astrophysics, and cosmology [1].

Fig. 1: Map of the LSST facilities in northern Chile on Cerro Pachón. Image taken from [32].

The LSST has determined a goal to achieve a wider-deeper-faster survey. Wider means to scan the area big as almost the whole sky. The Area will cover 30,000 deg^2 and ~ 20,000 deg^2 region and it will scan the ~1,000 times per 10 years. The single visit exposure time will be under 40 seconds. With all properties of the LSST, it would able to detect ~3 billion lensing galaxies, 10 million supernovas and to track the objects smaller than ~40 m per sample [3].

Table 1: The LSST base line parameters [2].

Quantity	Design Specification
Optical configuration	3 - mirror modified Paul - Baker
f-Ratio, aperture	f/1.234, 8.4 m
Field of view, etendue	9.6 deg2, 318 m2 deg2
Plate scale	0.2 arcsec/pixel
Pixel size, pixel count	10 μm, 3.2 Gigapixel
Wavelength coverage	320-1050 nm, ugrizy
Single visit depth	r~24
Single visit exposure time	30 sec (two 15 sec exposures)
Readout time	2 sec

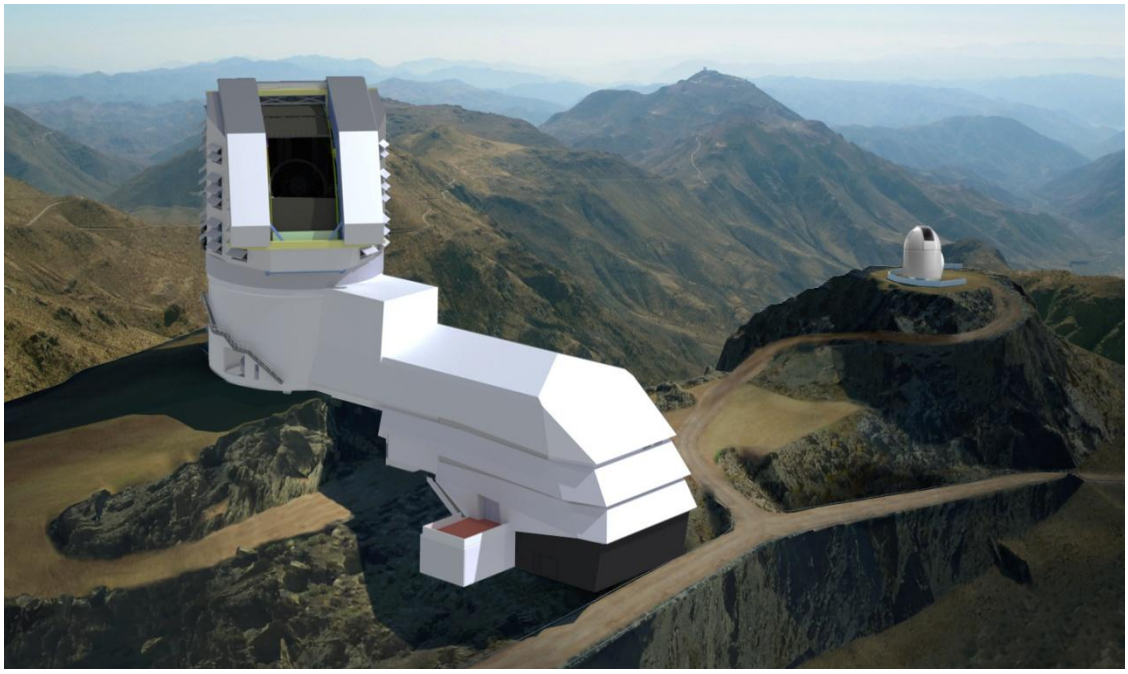

Fig. 2: The LSST facility on Cerro Pachón in Northern Chile [33].

2.1 Optics

The idea of LSST is to reach the widest possible field with the largest aperture (Fig. 3). With a large mosaic of sensors, it is a going to reach a large sensitivity. Only limits are the sky photon noise and the atmospheric seeing. This properties gives LSST a huge scientific potential. To achieve it the telescope is based on three mirror systems with optimization. The optic system contains a parabolic primary mirror convex spherical secondary mirror and a concave spherical tertiary mirror (Fig. 3). The result image is

formed between secondary and tertiary mirror. Spherical aberration is corrected by secondary mirror that is located at the center of curvature of the tertiary mirror. The telescope is extended by two mirrors to eliminate the effect of longitudinal and chromatic aberration [5].

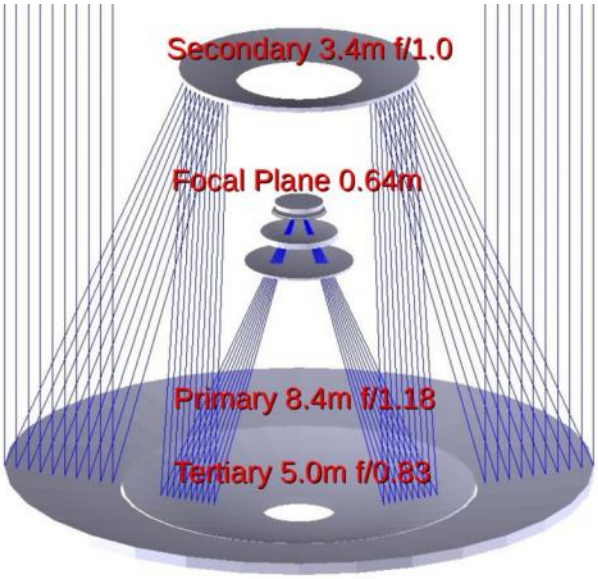

Fig. 3: The LSST optical design. The optic system is modified Paul-Baker three mirror system, where the LSST camera is placed at focal plane. This system provides uniform quality for capturing large field of view. Image taken from [34].

The LSST consist of large CCD platform (~3200 cm^2). This will minimize the number of gaps in final image mosaic. It is important to provide a fast readout of the entire focal plane and the actual readout should take 2 seconds. To achieve this goal, it is necessary to have multiple CCD outputs operating in parallel. As more parallel outputs modes per CCD are connected, the readout speed per output can be reduced to minimize the noise bandwidth. But with more output signal it is required to have more signal processing channels. Also, a segmentation provides the advantage to reduce the impact of bloomed charge from bright stars. Stars of 16th magnitudes and brighter will exceed the full pixel capacity, resulting in blooming up and down the column. The affected columns can be decreased by choosing appropriate segmentation. That leads to the blooming columns from the saturated stars can be approximately about 0.005% of the imaging area [5].

2.1.1 CCD Strawman design

For a camera was chosen it 4K x 4K format (see Fig. 4), to have the largest consistent result. The electronics were designed to be able to read out 500,000 pixels and allow to, get pixel readout rate of 250 kHz. Size of gaps between sub-arrays is around 100 mm [2].

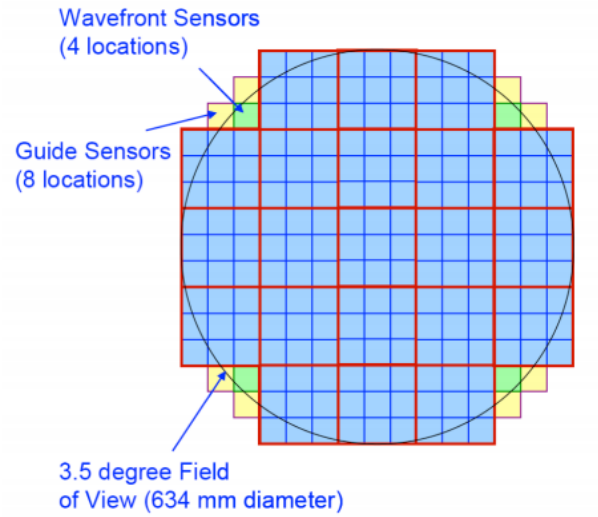

Fig. 4: The LSST 3.2-gigapixel focal plane array. Image taken from [17].

2.1.2 Focal plane electronics

The electronics supports CCD sensors matrix (4K x 4K) with 32 outputs ports per device. We can divide the electronics into “front end” and “back-end”. The front end electronics would process the output signal from CCD and provides clocks for the signal. The back end serves as a converter from analog to digital signal and buffer. The timing is important for the whole operation that means that the whole process needs to be synchronized in order of tens of nanoseconds. The structure of front and end electronics is the “raft based” (Fig. 5). Ine raft is equal to 3 x 3 array consisting of 32 segments of total 288 CCD output ports [6].

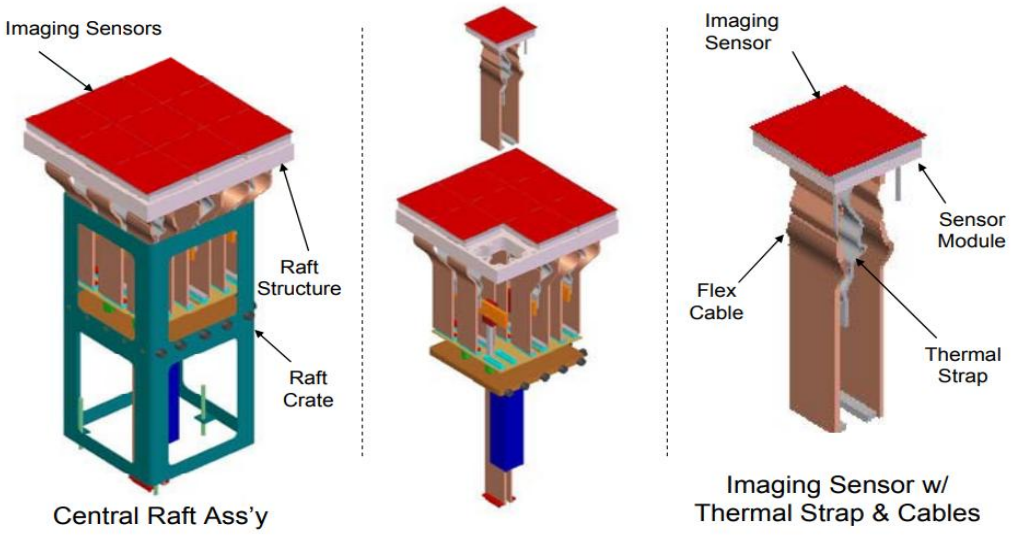

Fig. 5: Raft module with imaging sensors, front-end electronics and thermal connections.Image taken from [6].

2.1.3 CCD Packages

The support structure for sensor chip is made of materials with very low-temperature expansion coefficients. Materials like aluminium nitride and invar. The sensor is glued to an aluminium nitride substrate. To aluminium nitride substrate and photon-sensitive silicon are connecting bond wired to make the electrical connection [6]. The proper scheme is shown in the Fig 6.

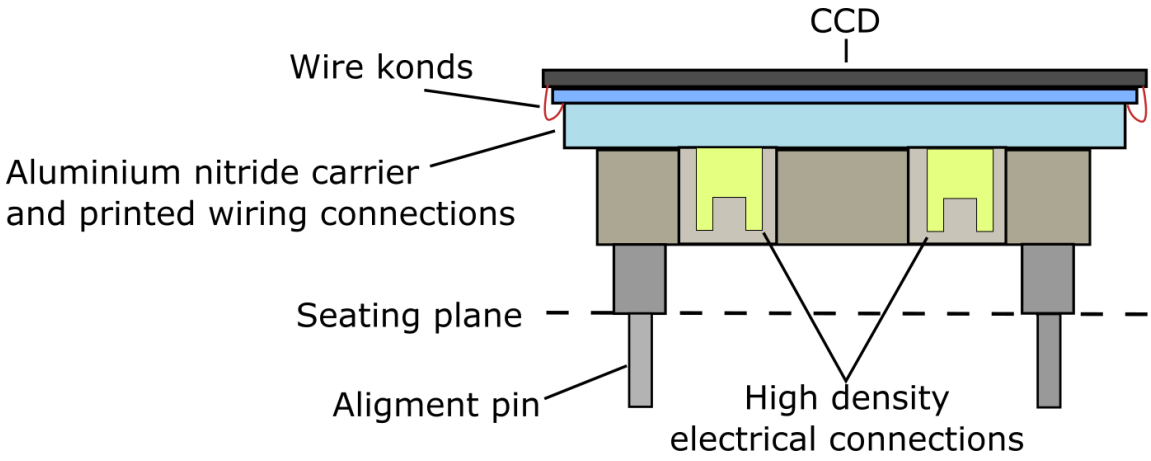

Fig. 6: CCD on aluminium nitride carrier with mechanical and electrical parts. Modified from [6].

2.1.5 Colour filters

The LSST consist of standard astronomical filter set – u, g, r, i, z, and Y bands [29]. Full Width Half Maximum (FWHM) transmission we can find in table 2 [6].

Table 2: The LSST baseline of filter band-pass FWHM [6].

Filter	λ_1	λ_2
u	330	400
g	402	552
r	552	691
i	691	818
z	818	922
Y	970	1060

2.2 Mechanical design of LSST camera

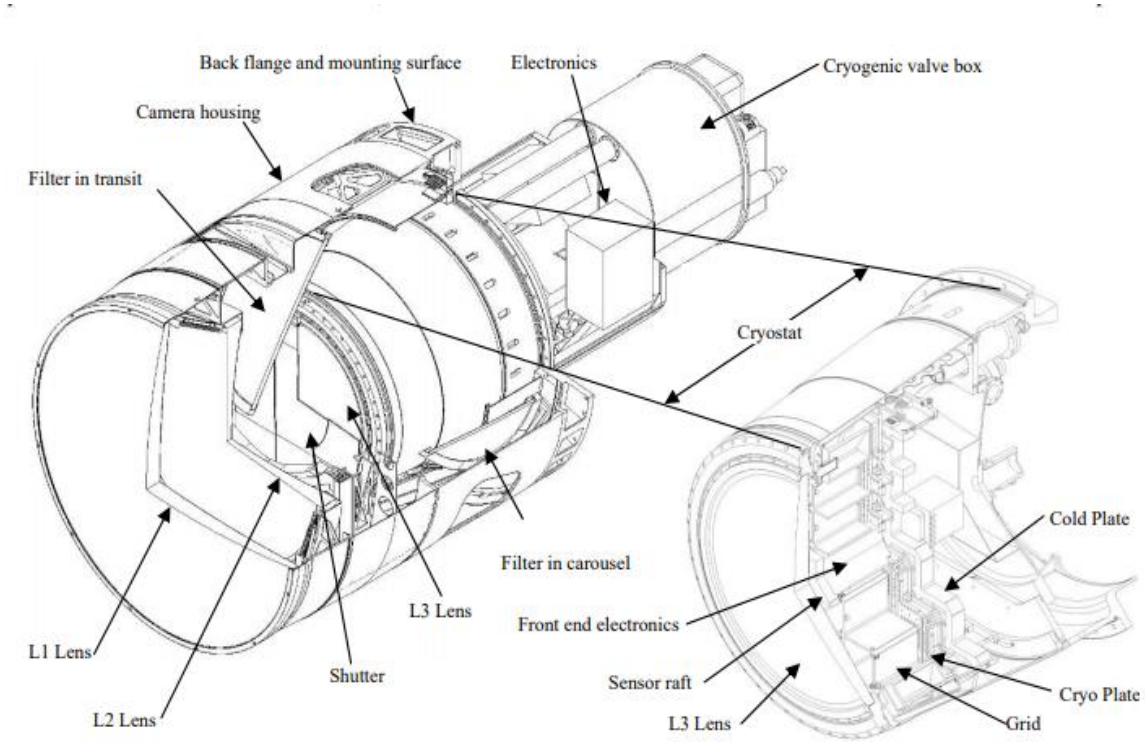

Fig. 7: Schema of the LSST Camera (left) and cryostat and it sections. Image taken from [2].

The camera has fully unclosed and self-contained design (Fig. 7). The Design itself consists of a housing that will hold 3,000 kg of equipment and mechanical parts. Inside, whole housing is inside a vacuum. Those conditions are made for CCD detectors that operate at temperature t = -100 °C. Also, it helps the readout electronics to turn down the noise [2].

2.2.1 Cryostat structural support system

To create low temperature, the LSST has Cryostat structural support system. The cryostat structural support system is made by components that support CCD sensors rafts in the vacuum that is made by cryostat. Components contain the cryostat housing, grid structure and support flexures and the kinematic coupling interface to the sensor rafts. It is important for the cryostat structural support system to hold the CCD sensors flat on the focal plane to precisions of 10 microns. To achieve this requirement the system needs to be isolated from the external disturbances such as a different thermal condition that could affect the structure [2].

2.2.3 Grid design

The LSST will remain in the movement most of the time, it is important to remove any distortion that could affect the flatness of CCD´s on the focal plane. That means that the Grid needs to be very stiff but also needs to remain open and allow to an installation of the sensors rafts and electronics. TheGrid is made of a silicon-carbide ceramic matrix composite. This material is mostly used in aerospace industry for his lightweight and structural stable properties [2].

2.2.2 Kinematic coupling

Kinematic coupling known as a Maxwell mount (more referred to as a three-vee mount) is the first part of isolation and it is located at the interface between the sensor rafts and the Grid (see subsection below). The Position of vees is in a raft of silicon-nitride ceramic balls that are fixed in cups mounted to the Grid. This design is perfect for a kinematic connection that can reduce distortion and it can create tolerances for assembly and to help control of thermal motion during cooling down the process [2].

2.2.4 Cryostat thermal system

The cryo plate and the cryo shroud are the main parts of the cryostat thermal system. The cryo plate supplies the heat sink for the sensor front for the electronics for CCD sensors, and for electronics modules. The cryo plate is placed directly behind Grid with thermal isolation. The cryo shroud is placed and thermally grounded to the perimeter of the cryo plate. The whole Grid is surrounded by cryo shroud. Cryo plate is cooling the

shroud to which support multi-layer insulation (MLI) makes a radiation barrier inside of the warm cryostat wall [2].

This design of the cryostat components is important for sensors functionality. The CCD sensors must have the stable operating temperature up to 0.3 K. The quantum efficiency of the detector heavily depends on temperature and must be stabilized to eliminate errors. Temperature needs to stable even for the Grid itself. The small changes in the average grid temperature can affect the whole system by the thermal Grid distortion that can move the sensors out of their required flatness on the focal plane. The system requires parallel, thermal paths, that allow conductive cooling for the front end electronics, and thermal grounding for the Grid, that can control the temperature of each raft independently and can stabilize CCD temperatures over time [2].

Cryostat consists of four separate thermal zones. The Cryo Plate and shroud are coldest thermal zones with the temperature being t = -120 °C. The CCD on the focal plane is on the second thermal zone, to reduce the cryo-pumping load on the CCD′s. The third thermal zone is for a grounding of the power, clock and digitizing electronics for each raft and there is the temperature of t = -40°C. The fourth thermal zone stays warm to keep metal and glass surface warm, to reduce the gas load and the chance of contamination. These four zones are controlled independently. This helps to protect the optical surfaces during cool-down and warm-up sequences [2].

2.2.5 L1/L2 assembly

The LSST will contain two large lenses (L1 and L2) that are housed at the front end of the camera. The first lens L1 has a clear aperture radius of 775 mm and the second lens L2 smaller than L1 but still large and heavy, has a clear aperture radius of 551 mm. The design of the assembly is important for all future operations. There are special requirements for design. First, during the telescope re-points and camera rotation, lenses must remain stable. A Motion of the lenses, cause a quality degradation of the images. Compensation for is a hexapod positioner but it can compensate only some motion. Second, the whole support structure has to be lightweight. The lenses are mounted at the end of the camera that causes the offset for response to dynamics of the system. Thus, mass must be optimized while it must provide stiffness and [2].

2.2.6 Filter exchange system

The LSST camera houses five filters that can be changed during operation. The Maximal number of exchange time is less than 120 secs. This time is important to maximize each image taking during the night. During one night there will be 10-15 filter changes that is 5% of the viewing time. Filters that are not in use are hold by the carousel that also moves filters into position. The filters are mounted to cradles on a ring that surrounds the cryostat. The mechanism grabs the filter that placed in a slot, then it moves it forward and pivots into final position before L2 lens. There is also manual changer that is used for swapping out a filter during daytime access [2]. Scheme of filter exchange is shown in Fig. 8.

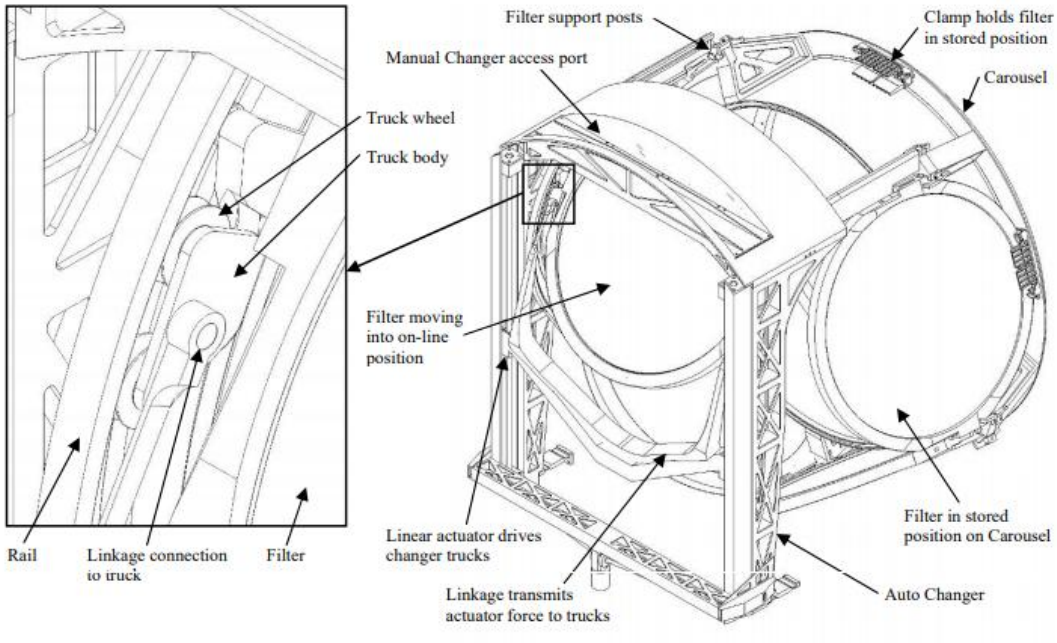

Fig. 8: Filter exchange system and his parts. Image taken from [2].

2.2.7 Shutter

The shutter consists of three flat blades that move across the focal plane to begin or end the exposure. Main requirements for the shutter summarized are in table 4. Mechanical design must allow tight control of exposure time across the entire field of view. The three blades are made of carbon-fiber face sheets and a high-density foam core.

The blades are driven from one end and they are supported by separate carriages on the single rail [2].

Table 4: The Shutter parameters [2].

Property	Value
Minimum exposure time:	1 sec
Opening/closing time:	0.5 sec
Exposure time uniformity:	100 m-sec
Max shutter thickness:	19.1 mm
Cyclic lifetime:	107 cycles

2.3 Science goals for LSST

There are four main science topics that LSST will focus on. The first topic is studying Dark Energy and Dark matter. This research could help us to understand a process of expansion of the Universe and its acceleration. The second topic is about mapping the Solar System and making an Inventory of Solar System (For example to observe Pluto-sized objects). The third is to explore and analyze the Transient Optical Sky. There are many objects that are not explored yet and need to be mapped. The fourth and last main topic is mapping the Milky Way [1].

As ground-based telescope the LSST has imagining limits. The practical field-of-view of the telescope is limited by atmosphere turbulence but the LSST filed-of-view area is maximalized to the practical limit 9.6 deg^2 [2]. The LSST base line parameters are summarized in table 1.

2.3.1 Dark energy science

In 1998 was observed that universe is accelerating [23]. This was measured by using distance measurement of Type Ia supernovae. Later in 2011 was awarded Nobel Prize in Physics for this discovery. This breakthrough is the challenge for current theories of cosmology and fundamental physics [1].

Studying and understanding dark energy (DE) is one of the major topics in cosmology and it is important for future research. The LSST team created Dark Energy Science Collaboration (DESC). DESC cover around five studies of dark energy:

1. Weak gravitational lensing (WL) – a measure of specific distortion of background image caused by a light bend that passes thought galaxies or cluster galaxies. WL is important for LSST because it is sensitive to dark energy. This effect depends on the angular-diameter distance given by redshift relationship and rate of structure growth [21].
2. Large-Scale Structure (LSS) – detection of the large power spectrum to get a distribution of matter as a function to determine redshift. This procedure also contains the Baryonic Acoustic Oscillation (BAO) measurement of the distance-redshift relation [1].
3. Type Ia Supernovae (SN) – detection of distances by luminosity and determination function of redshift where Type Ia SN is used as standardized candles [1].
4. Galaxy clusters (GC) – survey to measure structural density, distribution of galaxy cluster to determine function of the redshift [1].
5. Strong gravitational lensing (SL) – measuring of the angular displacement capturing of time delay of foreground object to create multiple images of source object [1].

Besides those five probes, there are other important tasks relayed to DESC. The tasks consist of topics such as creating data and computing models for DE science, simulations that will address main five probes and technical operations as calibration for survey tasks [1].

The important part of the DESC is simulations and modeling situations to determine capabilities of the LSST in describing dark energy. In some cases, LSST must reach three orders of magnitude improvement in PSF (Point-Spread Function). To achieve these goals. it is necessary to create high-fidelity simulations that would cover the properties and cosmological measurements. These steps are important for the development of correct strategies and algorithms. Block diagram of the process is shown in Fig 9 [1].

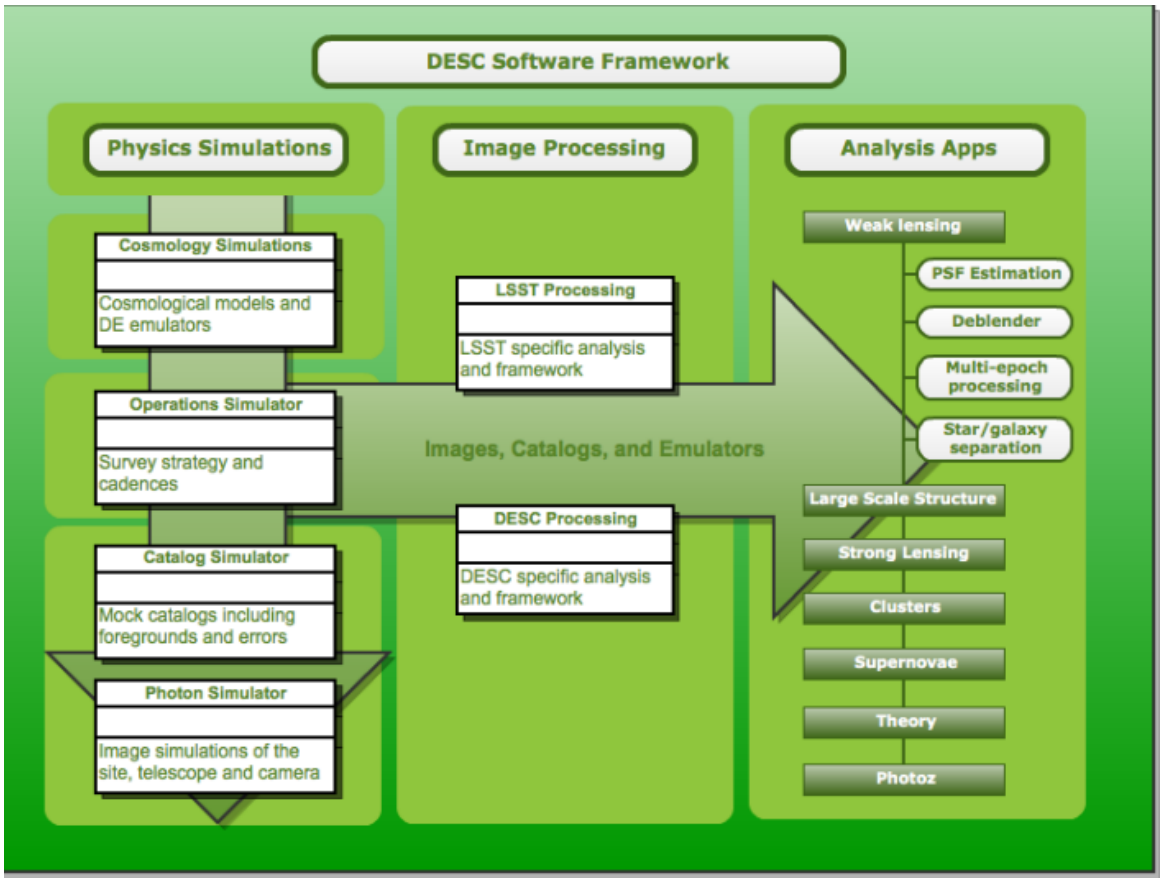

Fig. 9: DESC Software framework. Software framework is divided in three main parts – Physics Simulations, Image Processing and Analysis Apps. Every part has own subtopic. Arrows describe order of processing tasks. Image taken from [1].

2.3.2 Mapping the Milky-way

Milky-way was always a point of interest for observation. LSST will focus on the structure of Milky-way galaxy and its neighbours. It will specify construction and inventory of Solar system that includes everything from Earth to asteroids in Kupier Belt (Planetesimal disk created by the relic of evolving Solar System [20]). This also includes Milk way science. Beside this mapping, it also helps to detect hazardous asteroids that could be the threat for the Earth [7].

There is a partnership between Gaia and LSST that helps to increase the efficiency of the observation. The LSST will give an extension of Gaia data to expand and update its astrometric catalog [24]. On the other hand, Gaia will help to get a higher quality of astrometric measurements.

The observation plan for LSST has a goal to scan full sky during 3 nights. During one night there will be around 10 million time domains events that allow extending catalog

of orbital elements for around 6 million bodies in the Solar System, a catalog of objects for 37 billion objects (20 billion galaxies, 17 billion stars) [7].

2.3.3 Exploring the Optical Transients

Nowadays scientist focuses on measurements of gravitational lensing, discovering of supernovae, trying to understand Gamma-Ray Burst sources and other topics that are important in astrophysics. The LSST will focus deep limiting magnitudes that would lead to rare and exotic objects (neutron stars black hole binaries, stellar flares, etc.). The LSST will enable the large survey to detect a large number of microlensing events in the Local Group (group of two large galaxies – the Milky Way and M31 and smaller galaxies [25]) and perhaps more. For these discoveries it is important to cover a large area to increase the chance of rare detection events, there are special requirements for measurements such as good time sampling to determinate light curves accurate measurement of wavelengths to classify variable objects and more. The LSST is going to probe night sky for ten years that allows much large area scan of the sky. With rapid cadence, imaging can even capture eclipses in ultracompact double degenerate binary systems [19].

2.3.4 Solar system

The LSST observation will focus on objects brighter than 16th magnitude and also plains deliver information about small body observation and detection. During 10 years LSST catalog over 5 million Main Belt asteroids, around 300,000 Jupiter Trojans over 100,000 Near Earth Objects (NEOs), over 40,000 Kupier belt objects (KBOs), tens of interstellar objects and over 10,000 comets. The LSST Solar System Science Collaboration (SSSC) set four priorities to focus on [18].

- Active objects
- Near Earth Objects (NEOs)
- Inner Solar Systém
- Outer Solar System

3 Charge-coupled devices

Chargec-coupled devices also known as CCDs were invented in 1969 at Bell Laboratories [26]. We can find CCDs in some cameras or camrecoders. The CCDs are being used in special application as science experiments and military surveillance [8].
We can divide CCD into two types by array dimension exactly or 1-D arrays and 2-D arrays. The 1-D arrays consists of single-only photodiodes and 2-D arrays are multiple lines with same snes [15].
The basic part of a CCD is the MOS (metal oxide semiconductor) capacitor (silicon substrate), a dielectric film (oxide) and a conductive gate. The Dielectric film is usually SiO_2 and sometimes it can be a combination of other materials. The thickness of the film is about 0.004 μm to 0.05 μm [8].

CCD consists of rows of closely spaced electrodes that are separated from a semiconductor substrate by a thin oxide layer. Each electrode is connected to the own bias voltage. Inside semiconductor, there is depletion region where a potential well can store the electrical charge. If a bias voltage is applied to an electrode, the potential well is made. By making a proper sequence to the electrodes, the electric charge can be moved through semiconductor (shown in Fig 10). The sequence is set by the clock. The clock is specific for each type off CCD and it can be found in producer's documentation called the timing diagram [15].

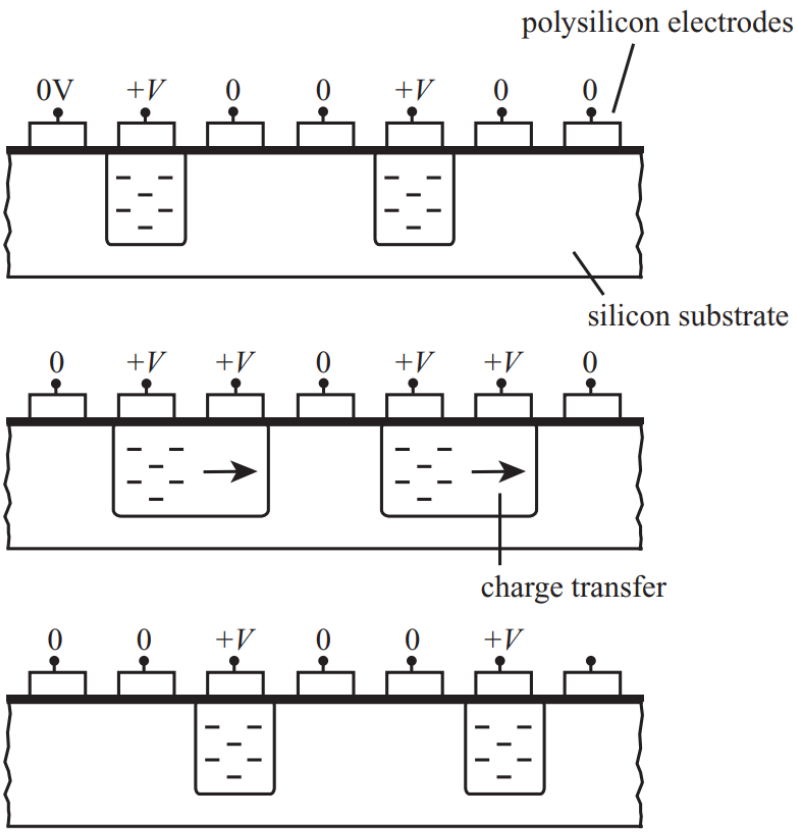

Fig. 10 Diagram of CCD readout process. Image taken from [27].

3.1 Types of CCD sensors

3.1.1 Interline- transfer CCD (IL-CCD)

The main difference between CCD and IL-CCD is that every pixel has its own photodiode that converts photons to electron-hole pairs and owns register. When IL-CCD (Shown in Fig. 10) captures photons and converts them. Electrons are transferred from a photodiode to readout registers. After readout from vertical registers, the charge is transferred to the horizontal register through an output amplifier and read out from IL-CCD [10].

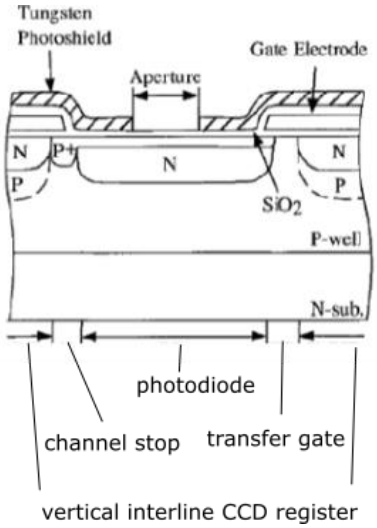

Fig. 11: Illlustration of IL- CCD pixel image. Edited from [10].

3.1.2 Full-frame CCD (FF- CCD)

The FF-CCD consist of a shutter that shades sensor from light. As a photon is detected, shutter closes and charge integration and transport are done in that specific pixel. The cross-section is shown in Fig. 11. [10].

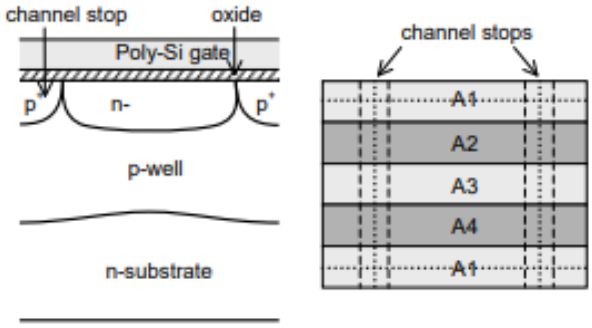

Fig.12: The cross section of FF-CCD pixel (left) and top view of four-phase image pixel (right). Taken from [10].

3.1.3 Backside illuminated CCD

The Backside illuminated CCD consist of paging array (5-15 microns thick) and silicon with a highly doped substráte material. When sensors capture light from the back surface it generates free electrons. Electrons are shifted by drift and diffusion process into the buried channel [27]. The cross-section is shown in Fig. 13.

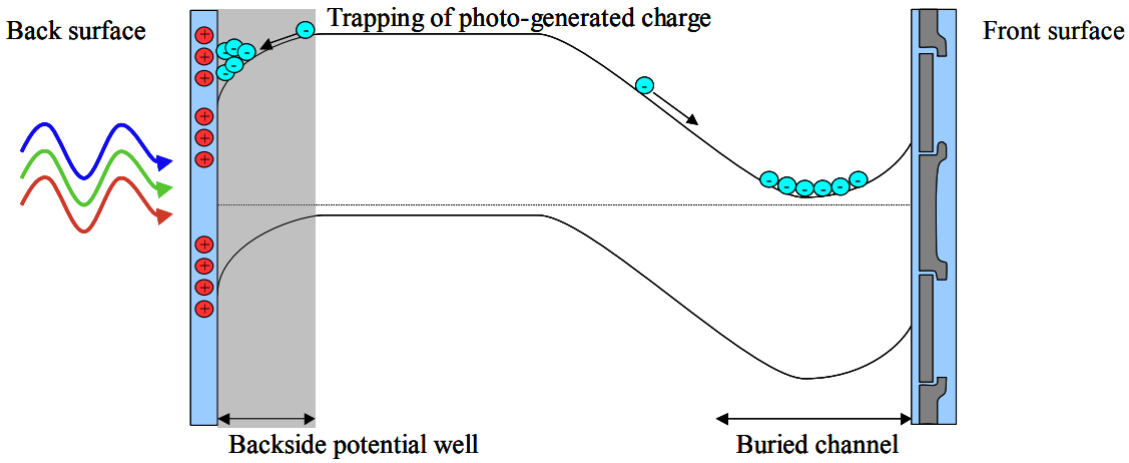

Fig. 13: The cross section of Backside illuminated CCD. Taken from [27].

3.2 CCD Properties

In imaging system as CCD missing data artifacts are the common phenomenon. How CCD age the more defects appear likely [11].

3.2.1 Quantum efficiency

Quantum efficiency (QE) can easily decrease with these factors: reflection loss, incomplete charge collection, incomplete light absorption. Reflection loss depends on the antireflection coating used on the illuminated surface and on properties of the charge-collecting side. Charge collection will be near unity over most of the wavelength range, but with defects, on a surface, the collection causes degradation toward the blue end of the spectrum where is a big absorption that is near the surface. QE decreases with reflection losses for the red and near-IR region and multiple internal reflections will cause interference fringes as an optical response. This QE inefficiency can be reduced by proper sensor design and its processing. For uniform illumination, we can determinate QE η by equation:

$$\eta = \left[1 - \frac{\exp(-\alpha w)}{1+\alpha L}\right] T \qquad (1)$$

Where α is optical absorption coefficient, w is width of depletion region, L is the minority carrier diffusion length, T is stands for all reflectance and transmission process [12].

3.2.2 Full well capacity

Full well capacity is described as the amount of charge a pixel can hold in routine operation. For example, a Kodak CCD with 9-micron pixels (9 microns on a side for a projected area) operates in MPP (massively parallel processing) mode has full well capacity 85,000 electrons per pixel. For comparison, a SITe CCD with 24-micron pixels can provide a full-well capacity of 350,000 electrons per pixel [15].

3.2.3 Dynamic range

Dynamic range is determinate by full-well capacity and readout noise [16]. It specifies the measurable range of a sensor as the maximum level to the minimum level of the detection. The value is set as:

$$\text{Dynamic rage} = \frac{\text{Saturation charge}}{\text{Readout noise}} \tag{2}$$

or can be given as

$$\text{Dynamic rage} = 20 \cdot \log\left(\frac{\text{Saturation charge}}{\text{Readout noise}}\right) \text{ [dB]} \tag{3}$$

Dynamic range can change depends on operating conditions as operating temperature and integration time. The lower detection limit can be observed during room temperature conditions. This is result of dark current if the sensor is cooled the dark current can be ignored and dynamic range is determinate by readout noise [30].

3.2.4 Pixel capacity

Pixel capacity depends on the size of a pixel on CCD, with a larger pixel comes larger capacity. The capacity is limited, and if it exceeded while capturing the light the pixel becomes saturated, and electrons can spill into same columns of pixels. For comparison, Kodak KAFI400 (6.8 X 6.8 μ pixels with MPP (Massive Parallel Processing) technology) has 45,000 electrons per pixel, and on the other hand, Thomson 7863 and 7883 (23 X 23 μm pixels with traditional technology) has 940,000 electrons per pixel [9].

3.2.5 CCD Quality

It is impossible to create perfect CCD sensors without any faults. Every CCD must be tested before actually using. The final evaluation helps manufacturers set into classes to define CCD's quality. Every fault affects the whole final image. Kodak describes types of faults and divides them into three groups. The first group is called Point defects. Point defects are pixels whose signal has 6% difference than adjacent illuminated pixels on 70% of saturation. The second group is Cluster defects are a group of maximum five pixels that are defective. The last group is Column defects. That means a group of defective pixels located in the same column [9].

3.2.6 The linearity of a CCD

The linearity of a CCD can be defined as the number of electrons that are generated in one pixel are proportional to photons captured by that pixel. At CCD the linearity is often better than 0.01 % but this limited by saturation of the CCD after saturation the linearity will change. This property can give the CCD no detection threshold it is only by limited if the number of produced electrons is less than image noise. The detector linearity can be used as for measurement of the luminosity that can be used in photometry. For example, to define luminosity of the comet, it is important to set reference points such as and measure number of electrons that were captured from comet and measure number of electrons that were capture from reference points and compare these sinals [9].

3.3 CCD Artifacts

3.3.1 Hot Pixels

Electron-hole pairs being generated by energy levels that are near midgap. This whole process increases dark current. Some pixel can generate high dark current near to dark rate. Every collision sequence can produce different amount of displacement damage even if protons have the same energy, it depends if a defect was created in the high electric field region, where can occur field-enhanced emission and result into a very large current [9].

3.3.2 Tree rings

Tree rings are artifacts that come from specific variation in the dopant concentration during the growth of the single-crystal silicon boule. Dopant variations are radially symmetric around the center of the silicon boule, and that causes small lateral electric fields. The result of this effect is space charge gradient. These fields allow the electrons to shift laterally, from the photon conversion to the gates at the back of the chip. This deviation is typically quite small, but it causes systematic biases in the measured position of objects based on the location where they are observed on the CCD. This electric field also distorts the shapes in observed objects while is the perpendicular axis undisturbed and the radial axis is stretched or compressed. This displays a measurable ellipticity to point sources, and without any proper correction (see Fig. 14), this effect can show as bias shear measurements and weak lensing effects [13] .

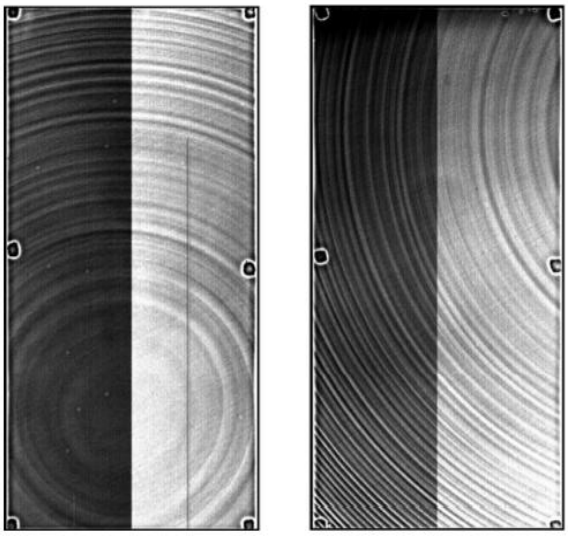

Fig. 14: Tree rings on masterdome flat images from the two DECan CCDs. Taken from [14].

3.3.4 Readout Noise

Readout noise (also read noise) is the amount of electrons capture pixel in final signal upon readout of the device. Read noise depends on two different processes. First is the conversion from analog to digital signal, this conversion also causes signal loses. Amplifier and A/D circuit that are on a chip will give us a statistical distribution of answers focused on mean value. In the hypothetical case of reading out the same pixel twice, each time with the same charge can give us a different result. The second

problem that causes read noise is electronics themselves. Depending on electronics parts that creates spurious electrons into final signal and puts random fluctuations in the output. When these two effects are combined the final values for every pixel are affected [15].

3.3.5 Defective pixels

Defective pixels are pixels with the wrong representation of the final signal. For example, dead pixels that cannot generate any electron proportion to captured photons. Defective pixels can be spread out in groups or columns. Amount of defective pixels is given by the manufacturer in document [9].

3.3.6 Dark current

Dark current can be generated without any light hitting the sensor. Electrons that are spontaneously generated are impossible to distinguish from electrons gathered from the light source. The Dark current depends on CCD temperature. During same temperature the sensors give same amount of electrons per time unit correlates with statistical dispersion linked to the probabilistic character. It can be decreassed by cooling down the sensor or create reference signal during exact temperature, hold sensors at the same temperature as during reference and subtract these two sinals [9].

4 Laboratory for CCD testing at IoP in Prague

4.1 Eletronics

Archon is CCD controller developed by Semiconductor Technology Associates, Inc (STA). The main features of Archon are receiving a signal from CCD and controls the whole process of capturing images from timing to loading final image. CCD captures image that is converted into an analog signal and sends them to Archon. The system receives configuration and sends data to a host PC. PC and Archon are connected via gigabit Ethernet connection. The CCD is connected to Archon via custom interface board [31].

Table 5: Archon Feature Summary. Taken from [31].

Compact size: 11.5” x 8” x 4.5” (29.21 x 20.32 x 11.43 cm)
Modular: 12 slots for ADC, clock driver, bias, heater, or other custom modules
Dense: Up to 4 ADC modules for 16 total CCD outputs
Low weight: 8.5 lbs (3.9 kg) for a typical 4 channel system
Low power: 41 W for a typical 4 channel system
High dynamic range: 108 dB at 100 kHz, 98 dB at 1 MHz using 16 or 32 bits per sample
Easy interfacing: standard gigabit network interface, either copper or fiber SFP module
On-board frame buffer: 2GB RAM for flexible readout
Timing core: 100 MHz master clock for 10 ns timing resolution
ADC Module: 4 fully differential AC-coupled 100 MHz 16 bit channels using digital CDS, and software selectable 1.33 V or 4 V input range
Clock Driver Module: 8 channels of 100 MHz 14-bit DACs for generating slew-rate controlled, multi-level clocks from -13.000…+13.000 V
Low Voltage Bias Module: 30 total biases at -14.000…+14.000 V, with 6 high power channels supplying up to 500 mA each (programmable current limit), and 24 low power channels supplying up to 10 mA each (1 A max total current per module)

The Archon consists of 32-bit CPU (Central Processing Unit), that provides high-level system configuration for a data. The CPU converts hot signals (bias, voltages, clock timing, etc.) into low-level commands for the FPGA (Field Programmable Gate Array) on each module [31].

4.2 Refrigeration equipment using liquid nitrogen

The laboratory contains two Dewar flasks where is liquid nitrogen stored. Dewar flasks are connected with vacuum chamber via a tube with electronic valve. On vacuum chamber sits vacuum tunnel part with a viewfinder and electronic connectors. Vacuum in vacuum tunnel part (VTP) is created by two pumps – turbomolecular vacuum pump HiPace 80 and membrane vacuum pump HiCube (shown in Fig. 16). The VTP is connected to Crycon 24C (Crycon). Crycon is temperature controller that scans the temperature of the area and holds the temperature. The scheme of the laboratory with equipment is shown in Fig 15.

4.3 Laboratory for CCD testing at IoP in Prague

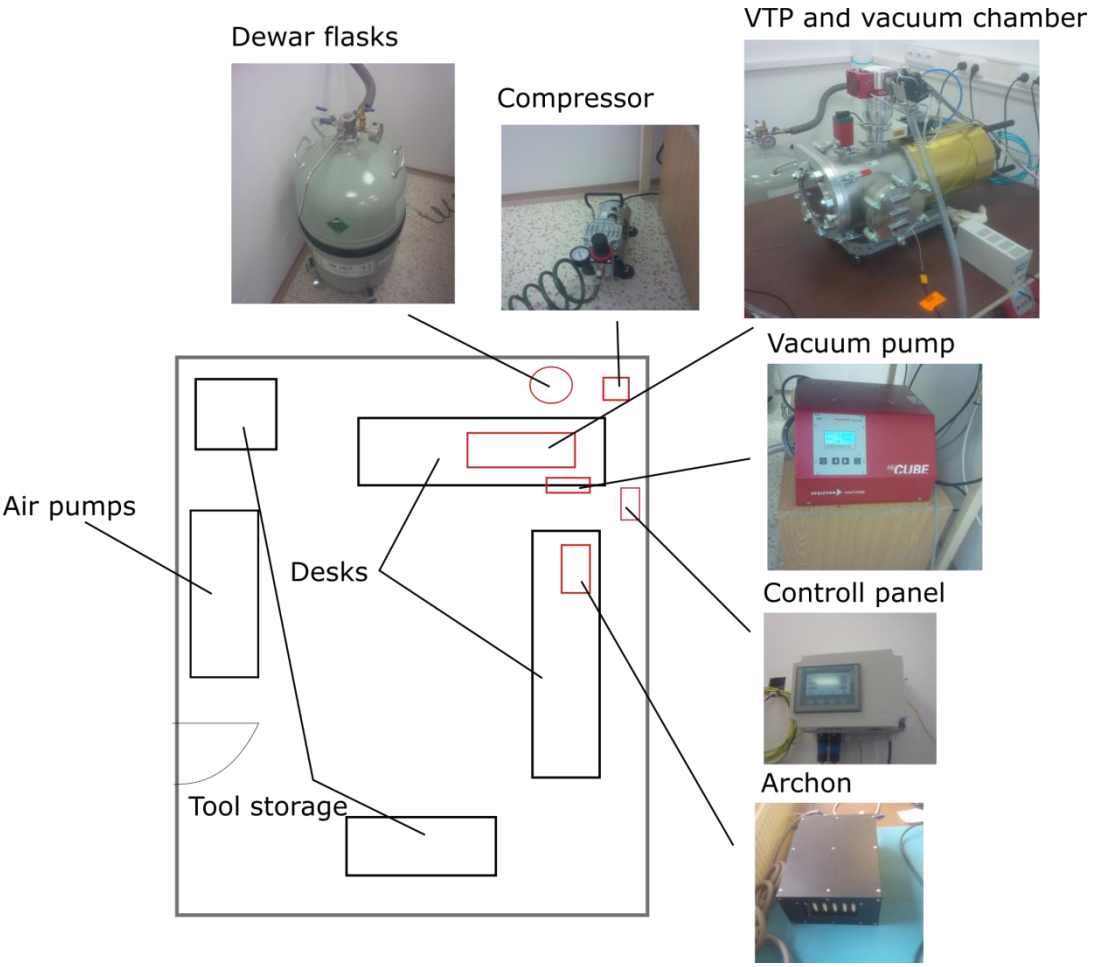

Fig. 15: Laboratory scheme with equipment

Whole laboratory is designed as a clean room. Which means that the windows are sealed and the dust is pressured out of the room by air filtering system, between entrance and laboratory there are three doors that have to be closed during measurement. There are air filters to reduce contamination of the air. The laboratory contains air condition to hold proper temperature during measurements. To eliminate short circuits that could destroy and or damage the device, the room is electrostatically grounded.

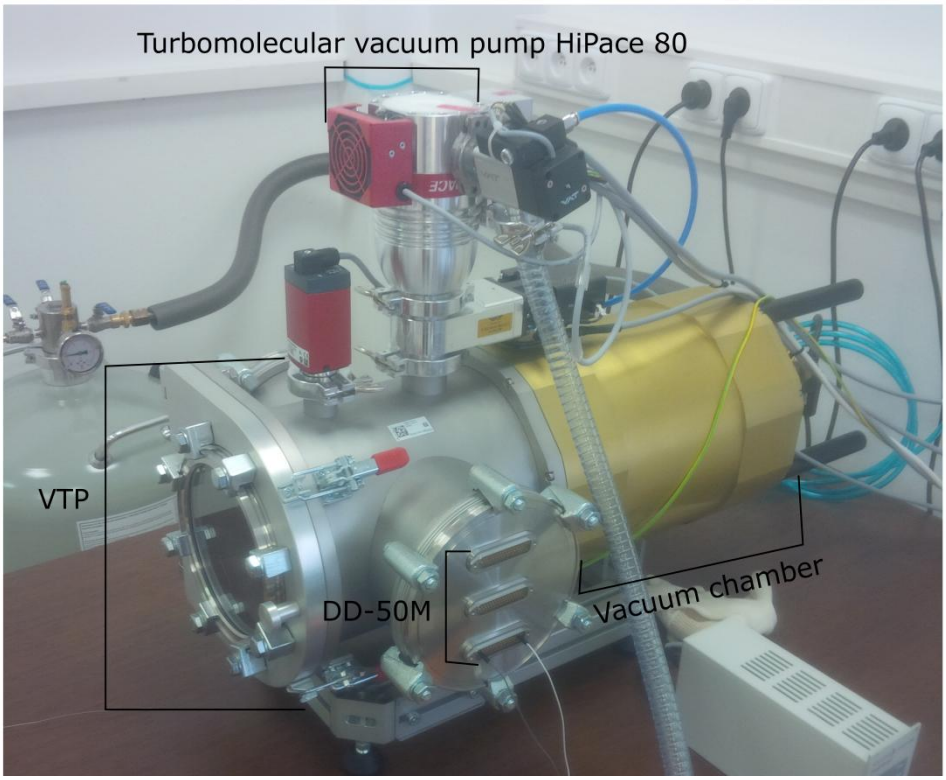

Fig. 16: VTP connected to vacuum chamber and turbomolecular vacuum pump.

5 Measurements at IoP in Prague

Measurements were done in the laboratory in Prague Institute of Physics (See Fig. 15). There were stable conditions during all measurements. For cooling, we used liquid nitrogen (LN). There are several safety rules when working in lab:

- wearing of special gloves when manipulating with LN,
- presence of at least two people,
- necessary caution to prevent spill of LN on clothing,
- grounding of all electrical devices via electrostatic board
- and no drink or food inside laboratory.

In this chapter there are results focused on the tests of Vacuum Chamber (VC). Describing a behaviour of VC was an important for three reasons. The first reason is to verify function of VC. Second is to check if there are no mechanical failures. And the third is to evaluate the behaviour of VC with a LN inside.

5.1 Preliminary test of thermal behaviour of Vacuum Chamber under room temperature

The vacuum chamber (VC) can be divided into two main parts – cover and container. Between cover and container, there is free space to reduce heat leaking over metal conduction. The temperature was measured on two spots of vacuum chamber as shown in Fig. 17. It was measured by two thermocouples types K (NiGr – Ni) that works at temperature range t = (-220 to 1372) °C ± 0.5 °C +2 % of measured value [35]. Thermocouples were connected to Greisinger GMH 3231 Series (GGMH) that displayed final temperature (shown in Fig 17). Thermocouples were attached to the front part of VC (shown in Fig. 17). The front part is supposed to be attached to VTP (Vacuum tunnel part) where is vacuum. During this experiment VC was not in vacuum and experiment was affected by room temperature.

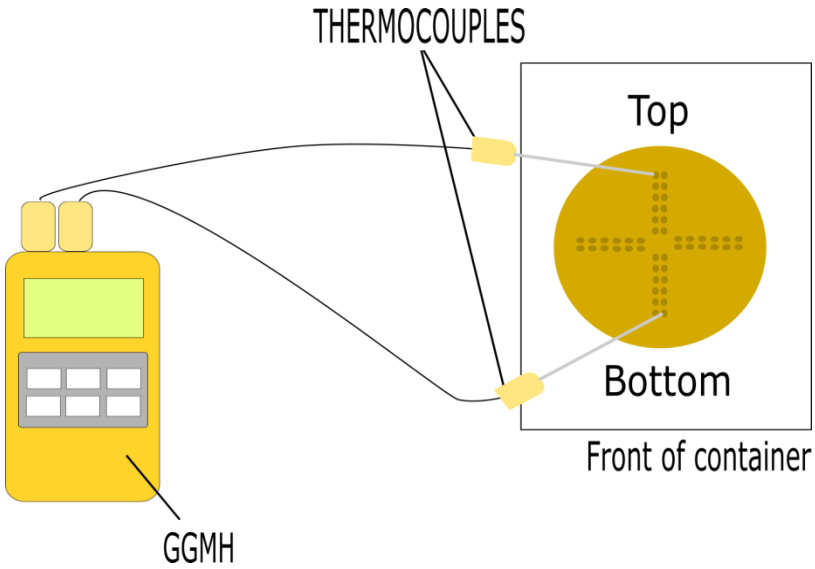

Fig. 17: Set up of temperature behaviour of vacuum chamber measurement.

Measurement started with temperatures of t = 21.6 °C for the top and t = 21.8 °C for the bottom place of coller. The cooling process lasted 290 seconds, where the temperature was t = -0.3 °C for the top and t = -9.3 °C. The difference in temperature is caused by two aspects. The first aspect is the flow of liquid nitrogen that is hitting the front part of bottom VC. This causes faster cooling of the bottom part (shown in Fig. 18). The second aspect is the cooling of top part of VC is caused by metal conductivity. This process causes temperature losses of conductivity and temperature could not spread equally.

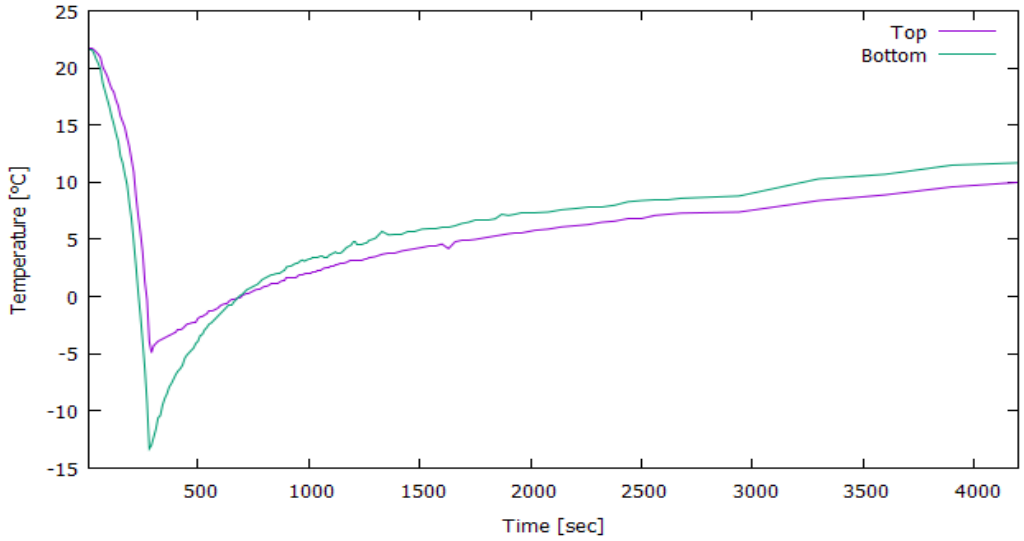

Fig. 18: Dependence of temperature on time during measurement temperature behaviour of vacuum chamber

5.2 Estimation of liquid nitrogen flow velocity

In this task, I had to estimate the consumption and speed of liquid nitrogen flow into the VC cooler. For calibration, we used a plastic box in shape of teapot with sizes 188 mm x 103 mm size. After pumping LN from a Dewar flask, the instrumentation starts to freeze. The measurements starts after LN gets a liquid form under lab temperature conditions. The teapot was filled for τ = 67 s (time was chosen randomly). The length between nitrogen surface and top of the teapot was Δl = 113 mm and that means the volume of nitrogen in the teapot was V = 0,52 l. We used formula We used formula $v = \frac{V}{\tau}$ (4). The result was v = 0.52 ls $^{-1}$ at pressure p = 1.2 atm in a Dewar flask.

5.3 Measurements of thermal conduction of Vacuum Chamber

The Dewar container has three parts – Dewar case, radiation shield, nitrogen vessel. To determine temperature in nitrogen vessel, you need to remove case and shield to have access. For removing you have to use hex keys to remove the screws. After that, it is important to measure the size of the vessel and determinate it volume and divide by

two to get half volume because we cannot fill the whole vessel the position will not allow it. The Position of a vessel has to be parallel with a table that allows nitrogen spill across the vessel. The vessel was filled with nitrogen under pressure p = 1.2 atm. The tubes where nitrogen flow was already cooled down from the previous experiment (determination speed of nitrogen flow), that explains the low temperature of tubes (Fig. 19). It also helps to cool down the vessel faster.

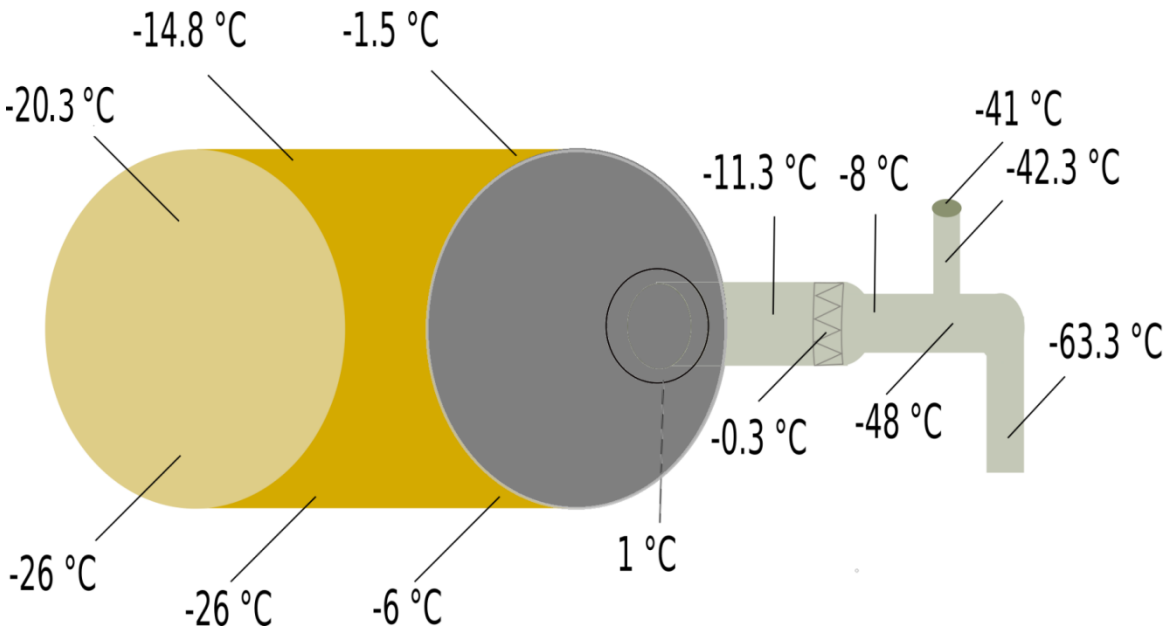

Fig. 19: Different temperatures on nitrogen vessel and tube

The result of temperatures was different on each part of the vessels and tube (Shown in Fig. 16). In Fig. 19 it is noticeable the bottom and front of the vessel have lower temperatures. This effect is caused by flowing liquid nitrogen under pressure that is hitting the front wall and bottom of vessel. The other places are cooler because of heat conduction. The vessel was uncovered and there is big temperature leakage. In future measurements, the vessel will be covered. The temperatures on the tube had higher differences on each part. Lower temperatures could be found between nitrogen exhaust and Dewar tube where LN flows and heat leakage is reduced by plastic foam cover. The section between exhaust and pipe's end had higher temperatures. This effect was caused by nitrogen steam that was coming back into exhaust and warming tube. This part of tubes also had not temperature cover.

5.4 Temperature measurement of nitrogen vessel in vacuum

The measurement can be divided into two tasks. The first task was to achieve a temperature t = -100 °C into VTP. The second task was to achieve the temperature of LN (t = -195.8 °C [22]). For both measurements was necessary to modify a measuring instrument - GGHM, to measure temperature into VTP. Access inside VTP is done by DD-50M connector that is on both sides of VTP. The thermocouple was placed inside VTP and connected via dupont cables with crocodile clips on the side that were connected to thermocouple and on the other side connected to DD-50M. GGMH was connected via dupont cables to DD-50M (Shown in Fig. 17).

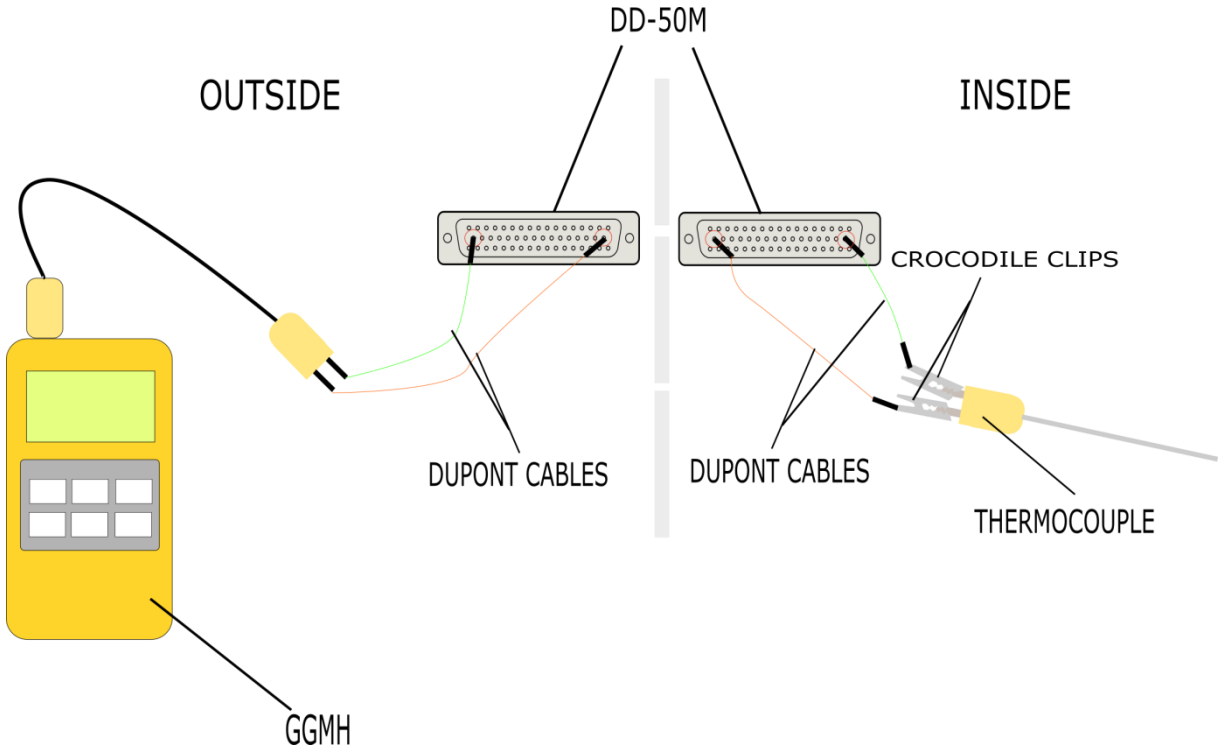

Fig. 20: Scheme of modified connection to measure temperature into VTP

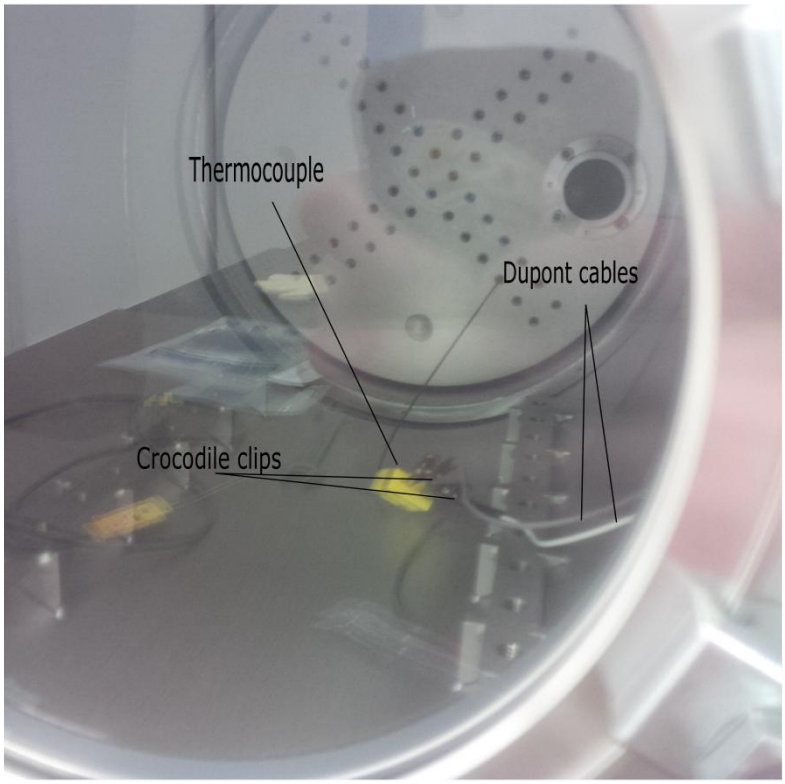

Fig. 21: Measuring thermo couple inside VTP

This extension created misleading output that had to be corrected. The correction was measured by the extended sensor (Fig.20) and without extension. For correction was measured two different temperatures. First was room temperature and the second was the temperature of liquid nitrogen in the teapot. This modification caused deviation of measurement. The deviation was caused by increasing electrical resistance, so the voltage that was delivered to GGHM was smaller than output voltage at end of the thermocouple. For this problem, it was necessary to correct data.

The correction formula was evaluated by measuring a room temperature and temperature of LN in the teapot. The measurement was done by modified connection (Shown in Fig. 17) and regular connection (the proper scheme shown in Fig.19). The room temperature was 22.2 °C, and temperature of LN was t = -180.7 °C. The result is a correction by equation $t_{real} = 1.138 \times t_{meas} - 5.88$ (5). The goal of tis measurment was to achieve -100 °C, because it will be stable temperature for sensor's cooling.

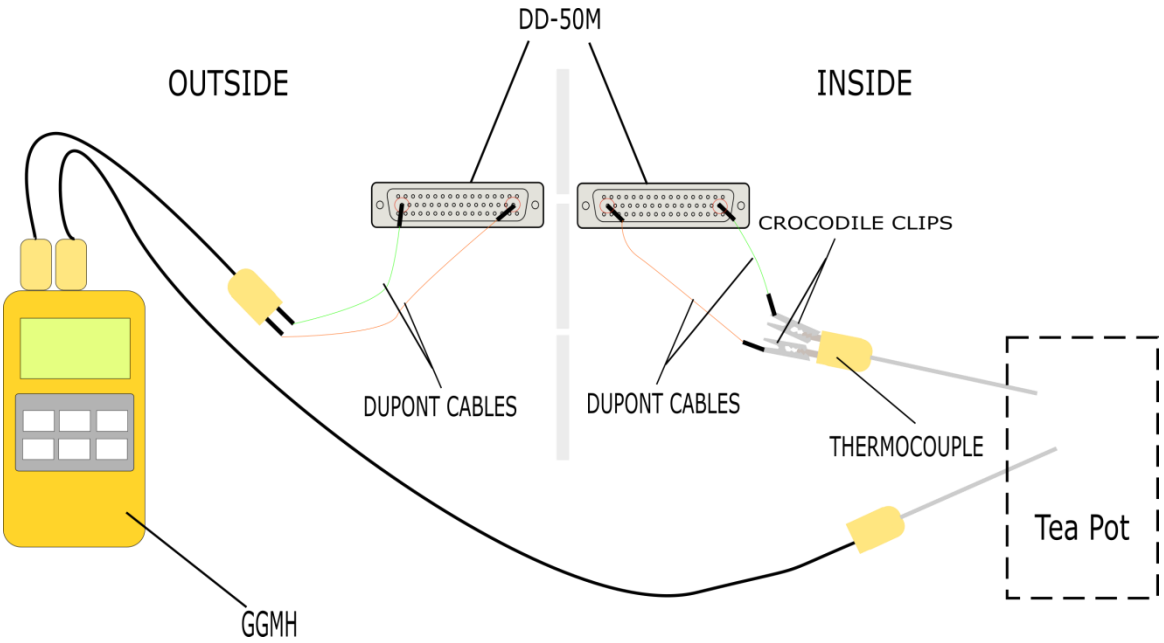

Fig. 22: Scheme of set up for evaluation formula

The progress (Shown in fig. 19) for both dependences (corrected and uncorrected) is practically same, only shifted towards y-axis. In the interval from 22.2 °C to 0 °C it is a noticeable delay that was caused by aperture without previous cooling after it was cooled down than the progress is almost linear.

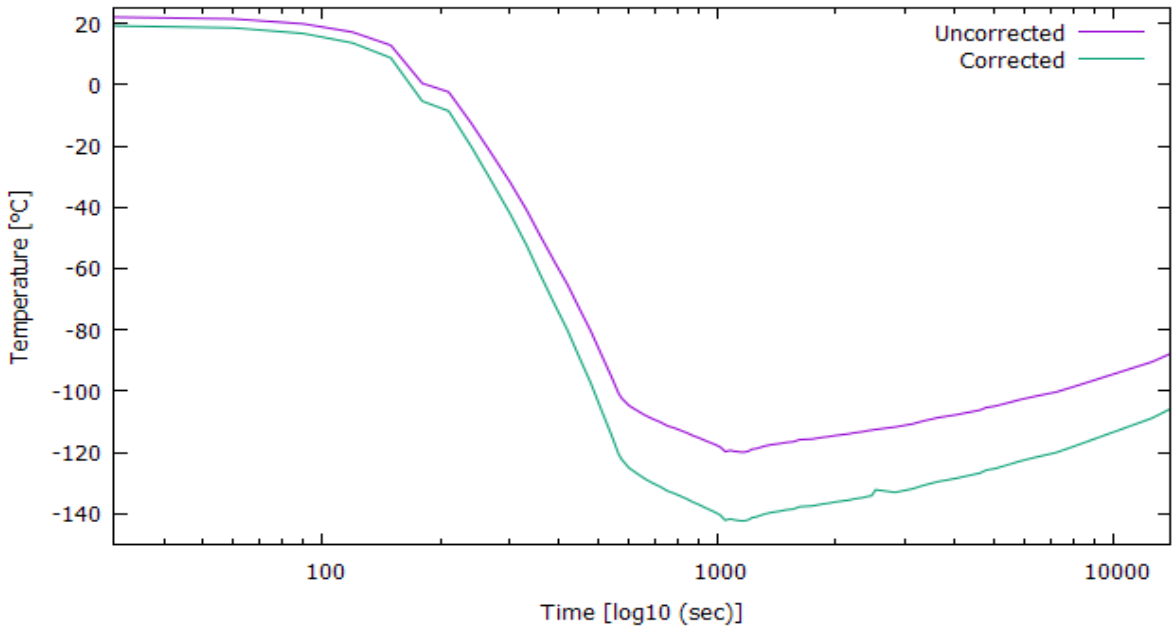

Fig. 23: Dependence og temperature on time with corrected data and without for first part of measurement

The second part of this was the measurement to achieve temperature -195.8 °C (temperature of LN [22]). The set up was used same as for previous measurement (Shown in fig. 17). The measurement started at temperature 11.9 °C. This temperature is lower than the room temperature. The vessel remained cooler after previous measurement and did not get back to the room temperature.

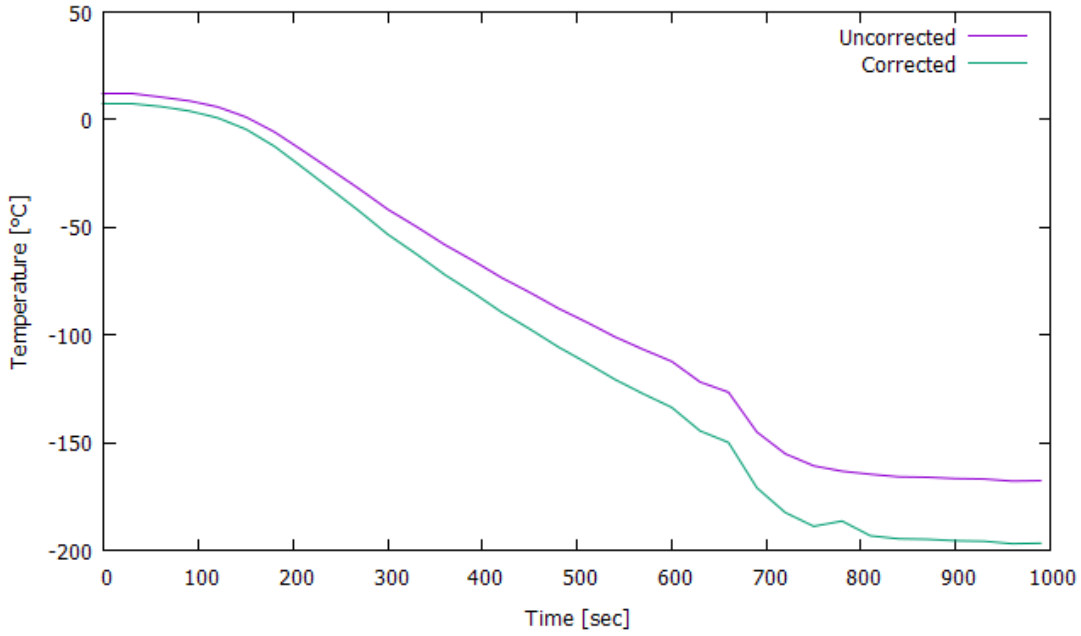

Fig. 24: Dependence of temperature on time with corrected data and without for second part of measurement

The temperature reached -196.95 °C. This temperature is higher than the temperature of LN, this is the effect is caused by inaccuracy of the measurement tool - GGHM and the correcting equation is not fairly accurate. To make equation more accurate it is necessary to gather more data for right evaluation.

The achieved results of measurements are discussed in the next chapter.

6 Data evaluation

6.1 Preliminary test of thermal behaviour of Vacuum Chamber under room temperature

This measurement was focusing on description of temperature behaviour in vacuum chamber. The cooling process was slow at beginning, because the pipe, where LN was flowing was not cooled. This caused time delay of cooling chamber. After pipes were cooled down, cooling was. The pumping was stopped at 4 minutes 50 minutes. The bottom was cooler than top. The reason is the VC was not filled enough and the heat was spread by thermal conductivity. After was the valve closed, cooling on both parts was continued. The bottom part stopped cooling after 280 secs at t = -13.3 °C at and the top part after τ = 290 secs at t = -4.9 °C. There is ten 10 secs time delay caused by thermal conductivity. The warming up process was slower, because only source of the heat was room temperature. The warming up process was faster at the bottom than at the top. This was caused by contact between an optic table and the bottom part of the vacuum chamber. The top part was in contact only with air. Heat conduction is faster in solid states than in gasses. This difference is no problem for future measurement because the front part of the VP will be in a vacuum.

6.2 Estimation of liquid nitrogen flow velocity

The NL flow depends on the pressure with higher pressure the speed of the flow is higher. The result was v = 0.52 ls^{-1}at pressure p = 1.2 atm. The second measurement was at the pressure in the Dewar container has the same setup like the previous measurement. The speed of the was v = 0.16 ls^{-1}

6.3 Measurements of thermal conduction of Vacuum Chamber

The differences on each part of the vessel share the same problem as the first measurement. The LN hits the front part of a vessel and makes it coolest on the whole vessel. The second coolest spot is a top part, where it is caused by thermal conductivity. The rest temperatures are lower because during thermal conductivity process causes

losses. On tube were lower temperatures, because the pipe was already cooled and flowing LN was cooling the pipe. The part of the pipe close to the vessel has higher temperatures than rest pipe it is caused by the vapours that were leaking out of the vessel and have a higher temperature than LN.

6.4 Temperature measurement of nitrogen vessel in vacuum

This measurement was done by only one thermocouple by in vacuum temperature was spread equally and the vessel was filled to its limit. The goal was to achieve t = -100 °C. This is temperature for cooling CCDs during a measurement. The temperature t = -100 °C was not corrected and actual temperature was t = -120.13 °C. The valve was closed at 585 secs, but cooling the vessel was continuing and reached t = -141.64 °C (corrected) at 1080 seconds. The next measurement was focusing how fast can be the vessel by cool down at t = -195.8 °C (the temperature of LN [22]). It was achieved a temperature t = -196.95 °C at τ = 960 secs. This temperature is higher than tabulated data. It is caused by inaccuracy of the GGHM and also the equation (3) was not fairly accurate. For accurate correcting equation is necessary to gather more data to do a proper statistic.

7 Conclusion

This bachelor thesis can be divided into three parts. The first part contains the description of the LSST project of its technical properties and major scientific goals for next ten years. The second part is focused on CCD sensors mainly about their technical properties and learning how to properly characterize them. The third and last part is dedicated to my own measurements at the laboratory at IoP in Prague. My task was to work with a vacuum chamber and liquid nitrogen cooling equipment. The vacuum chamber needed to be tested and described how it works in different conditions. These measurements are important for future CCD testing because vacuum chamber is the significant part of CCD cooling. First I needed to find out how chamber behaves during room temperatures and how liquid nitrogen affects the whole vessel. Also for this measurement, I had to determinate the speed of flow of liquid nitrogen to evaluate how much nitrogen is necessary to cool down the vessel. Last measurements were to determinate a speed of cooling of the front part of the vessel at the vacuum state. This measurement was important, because the conditions of this measurement are same as for CCD testing. The result of this measurement helped to a determine the standard operation of the vacuum chamber. It was found that the vessel works perfectly and it is ready to be used for high-end CCD testing. Also, the results are important for future upgrades of the whole system, such as the possible reduction of liquid nitrogen pumping into a vessel.

For future measurements, I would suggest creating the system that would evaluate the weight of vacuum chamber and opening or closing valve when it would be necessary to reduce nitrogen losses. My second suggestion is to program robotic arm that could place CCD on measuring place to reduce contamination a sensor and measuring place. Both additions will be controlled by the computer server that controls also the rest of the experimental setup. In this way, the proposed changes will significantly enhance the autonomous operation of the system, and the operators will be able to connect from home or office to control the whole set of measurements.

In the submitted bachelor thesis I learned about the LSST telescope, about the CCD sensors, about their importance in astronomy and about principles of their operations.

I participated in several measurement campaigns in the laboratory for CCD characterization at the Institute of Physics of the Academy of Sciences of the Czech Republic in Prague. My results have confirmed that the experimental setup is ready to host the high-end CCD sensors. Furthermore, during the future development of the experimental system, my conclusions might be used to optimize the operation of the liquid nitrogen cooling system.

List of the used sources

[1] ABATE, Alexandra, et al. Large Synoptic Survey Telescope: Dark Energy Science Collaboration. *ArXiv:1211.0310 [astro-ph.CO]*. 2012.

[2] NORDBY, Martin, Eli ATAD-ETTEDGUI, Dietrich LEMKE, Gordon BOWDEN, Mike FOSS, Gary GUIFFRE, John KU a Rafe SCHINDLER. *Mechanical design of the LSST camera* [online]. In: . 2008-7-14, 70182H- [cit. 2018-01-21]. DOI: 10.1117/12.790040. Dostupné z: http://proceedings.spiedigitallibrary.org/proceeding.aspx?doi=10.1117/12.790040

[3] RADEKA, Veljko, et al. LSST sensor requirements and characterization of the prototype LSST CCDs. *Journal of Instrumentation*. 2009, (4).

[4] LEE, James a J.Anthony TYSON. Toward Precision LSST Weak-Lensing Measurement. I. Impacts of Atmospheric Turbulence and Optical Aberration. *ArXiv:1011.1913 [astro-ph.IM]*. 2011.

[5] TYSON, J.Anthony. Large Synoptic Survey Telescope: Overview. *ArXiv:astro-ph/0302102*. 2003.

[6] GILMORE, Kirk, Ian S. MCLEAN, Mark M. CASALI, et al. *The LSST camera overview: design and performance* [online]. In: . 2008-7-12, 70140C- [cit. 2018-02-18]. DOI: 10.1117/12.789947. Dostupné z: http://proceedings.spiedigitallibrary.org/proceeding.aspx?doi=10.1117/12.789947

[7] RICH, R. Michael. The Large Synoptic Survey Telescope and Milky Way Science. *ArXiv:1712.02885 [astro-ph.IM]*. 2017.

[8] BURKE, Barry E. CCD Imager Development for Astronomy. 392. *Lincoln laboratory journal*. 2007, 16(2).

[9] MARTINEZ, Patrick. a Alain KLOTZ. *A practical guide to CCD astronomy*. New York, NY, USA: Cambridge University Press, 1998. ISBN 9780521599504.

[10] BOSIERS, Jan T. Technical challenges and recent progress in CCD imagers. Nuclear Instruments and Methods in Physics Research Section A: Accelerators, Spectrometers, *Detectors and Associated Equipment*. 2006, 565(1).

[11] CHUNG, Julliane, Matthias CHUNG a Dianne P. O'LEARY. Optimal Filters from Calibration Data for Image Deconvolution with Data Acquisition Error. *Springer's Journal of Mathematical Imaging and Vision*. 2011.

[12] ED. BY D.F. BARBE. WITH CONTRIB. BY W.D. BAKER ... *Charge- coupled devices*. Berlin [West] [u.a.]: Springer, 1980. ISBN 3540098321.

[13] BEAMER, Benjamin, Andrei NOMEROTSKI a Dmitri TSYBYCHEV. A study of astrometric distortions due to "tree rings" in CCD sensors using LSST Photon Simulator. *Journal of Instrumentation*. 2015, (10).

[14] PLAZAS, A.A, G.M BERNSTEIN a E.S. SHELDON. On-Sky Measurements of the Transverse Electric Fields' Effects in the Dark Energy Camera CCDs. *Publications of the Astronomical Society of the Pacific*. 2014, 126 (942).

[15] HOWELL, Steve B. *Handbook of CCD astronomy*. New York: Cambridge University Press, 2000. ISBN 052164058x.

[16] WALTHAM, Nick. CCD and CMOS sensors. HUBER, Martin C. E., Anuschka PAULUHN, J. Len CULHANE, J. Gethyn TIMOTHY, Klaus WILHELM a Alex ZEHNDER, ed. *Observing Photons in Space* [online]. New York, NY: Springer New York, 2013, 2013-10-11, s. 423-442 [cit. 2018-12-12]. DOI: 10.1007/978-1-4614-7804-1_23. ISBN 978-1-4614-7803-4. Dostupné z: http://link.springer.com/10.1007/978-1-4614-7804-1_23

[17] ABELL, Paul A., et al. LSST Science Book: Version 2.0. *ArXiv:0912.0201 [astro-ph.IM]*. 2009.

[18] SCHWAMB, Megan E. Large Synoptic Survey Telescope Solar System Science Roadmap. *ArXiv:1802.01783 [astro-ph.EP]*. 2018.

[19] IVEZIĆ, Žejlko, et al. LSST: from Science Drivers to Reference Design and Anticipated Data Products. *ArXiv:0805.2366 [astro-ph]*. 2018.

[20] LEVISON, Harold F, et al. Origin of the Structure of the Kuiper Belt during a Dynamical Instability in the Orbits of Uranus and Neptune Harold F. Levison. *ArXiv:0712.0553 [astro-ph]*. 2007.

[21] ALBRECHT, Andreas, et al. Report of the Dark Energy Task Force. *ArXiv: astro-ph/0609591*. 2006.

[22] MIKULČÁK, Jiří. *Matematické, fyzikální a chemické tabulky pro střední školy*. 4. vyd. Praha: Prometheus, 2007. Pomocné knihy pro žáky (Prometheus). ISBN 978-80-7196-345-5.

[23] GEISS, Adam. Observational Evidence from Supernovae for an Accelerating Universe and a Cosmological Constant. *The Astronimical Journal*. 1998, 116 (3).

[24] IVEZIĆ, Željko, et al. The Gaia-LSST Synergy. *ArXiv:1502.06555 [astro-ph.IM]*. 2007.

[25] FORBES, Duncan A, Karen L. MASTERS, Dante MINNITI a Pauline BARMBY. The Elliptical Galaxy formerly known as the Local Group: Merging the Globular Cluster Systems. *ArXiv:astro-ph/0001477*. 2000.

[26] BOYLE, W. S. a G. E. SMITH. Charge Coupled Semiconductor Devices. *Bell System Technical Journal* [online]. 1970, **49**(4), 587-593 [cit. 2018-02-18]. DOI: 10.1002/j.1538-7305.1970.tb01790.x. ISSN 00058580. Dostupné z: http://ieeexplore.ieee.org/lpdocs/epic03/wrapper.htm?arnumber=6768140

[27] HOENK, Michael E., Eustace L. DERENIAK, John P. HARTKE, et al. *Delta-doped back-illuminated CMOS imaging arrays: progress and prospects* [online]. In: . 2009-8-20, 74190T- [cit. 2018-04-20]. DOI: 10.1117/12.832326. Dostupné z: http://proceedings.spiedigitallibrary.org/proceeding.aspx?doi=10.1117/12.832326

[28] FARUQI, A. R. a Sriram SUBRAMANIAM. CCD detectors in high-resolution biological electron microscopy. *Quarterly Reviews of Biophysics* [online]. **33**(1), 1-27 [cit. 2018-03-19]. DOI: 10.1017/S0033583500003577. ISSN 00335835. Dostupné z: http://www.journals.cambridge.org/abstract_S0033583500003577

[29] FUKUGITA, M., T. ICHIKAWA, J. E. GUNN, M. DOI, K. SHIMASAKU a D. P. SCHNEIDER. The Sloan Digital Sky Survey Photometric System. *The Astronomical Journal* [online]. **111**, 1748- [cit. 2018-03-19]. DOI: 10.1086/117915. ISSN 00046256. Dostupné z: http://adsabs.harvard.edu/cgi-bin/bib_query?1996AJ....111.1748F

[30] *Image sensors*. Dostupné také z: https://www.hamamatsu.com/resources/pdf/ssd/e05_handbook_image_sensors.pdf

[31] *Semiconductor technology associates. Archon a high performance modular ccd controller*. 2016. Dostupné také z: http://www.sta-inc.net/wp-content/uploads/2013/08/Archon.pdf

[32] *LSST Summit Facilities* [online]. [cit. 2018-04-30]. Dostupné z: https://www.lsst.org/about/tel-site/summit

[33] *The world's largest digital camera is about to be built on top of a mountain in Chile -- here's what it will look like* [online]. [cit. 2018-04-30]. Dostupné z: https://www.businessinsider.com.au/worlds-largest-camera-in-chile-2015-9

[34] *LSST optical design* [online]. [cit. 2018-04-15]. Dostupné z: https://www.researchgate.net/figure/LSST-optical-design-The-telescope-design-is-a-modified-Paul-Baker-three-mirror-system_fig1_259708771

[35] *Bedienungsanleitung GMH 3230.* Dostupné také z: https://produktinfo.conrad.com/datenblaetter/125000-149999/125852-an-01-ml-GREISINGER_GMH_3230_SEK_DIFF_THERM_de_en.pdf

List of the used symbols and abbreviations

LSST - Large Survey Synoptic Telescope

CCD - Charge couple device

CMOS - Complemenetary Metal-Oxide-Semiconductor

IOP - Institute of Physics

CAS -Czech Academy of Science

NSF - National Science Foundation

DOE - Department of Energy

MLI - Multi-layer insulation

FWHM – Full width half maximum

L1/L2 - two large lenses

DESC - Dark Energy Science Collaboration

WL - Weak gravitational lensing

LSS - Large-Scale structure

BAO - Baryonic Acoustic Oscillation

SN - Supernovae

GC - Galaxy clusters

SL - Strong gravitational lensing

DE - Dark energy

NEOs - Near Earth Objects

KBOs - Kupier Belt objects

SSSC - Solar System Science collaboration

QE - Quantum efficiency

MPP - Massively parallel processing

A/D - Analog to digital

CPU - Central Processing Unit

FGPA - Field programmable Gate Array

VTP - vacuum tunnel part

VC - Vacuum chamber

GGMH - Greisinger GMH 3231 Series

LN - Liquid nitrogen

t – Temperature

τ – Time

Δl - Difference of a length

v -Speed of flow

V - Volume

p - Pressure

η - Efficiency

α - Optical absorption

w - Width

L - Minority carrier of the diffusion length

T – reflection and transmission process

List of figures